Characterizing Cell Adhesion by Using Micropipette Aspiration

Brenna Hogan, Avin Babataheri, Yongyun Hwang, Abdul i. Barakat, Julien Husson

Characterizing Cell Adhesion using Micropipette Aspiration

Brenna Hogan,[1] Avin Babataheri,[1] Yongyun Hwang,[2] Abdul I Barakat[1] and Julien Husson[1]*

[1] Department of Mechanics, Hydrodynamics Laboratory (LadHyX), Ecole Polytechnique, 91128 Palaiseau, France; [2] Department of Aeronautics, Imperial College London, South Kensington, London SW7 2AZ, UK

Abstract

We developed a technique to directly quantify cell-substrate adhesion force using micropipette aspiration. The micropipette is positioned perpendicularly to the surface of an adherent cell and a constant-rate aspiration pressure is applied. Since the micropipette diameter and the aspiration pressure are our control parameters, we have direct knowledge of the aspiration force, while the cell behavior is monitored either in brightfield or interference reflection microscopy. This setup thus allows us to explore a range of geometric parameters, such as projected cell area, adhesion area or pipette size, as well as dynamical parameters such as the loading rate. We find that cell detachment is a well-defined event occurring at a critical aspiration pressure, and that the detachment force scales with the cell adhesion area (for given micropipette diameter and loading rate), which defines a critical stress. Taking into account the cell adhesion area, intrinsic parameters of the adhesion bonds, and the loading rate, a minimal model provides an expression for the critical stress that helps rationalize our experimental results.

Received date XXX

*Correspondence: julien.husson@ladhyx.polytechnique.fr

KEYWORDS

Micropipettes, Endothelial Cells, Cell Adhesion, Interference Reflection Microscopy, Force Spectroscopy, Detachment Force.

INTRODUCTION

Cell adhesion is involved in a plethora of physiological and pathological cellular processes, and cell substrate adhesion affects several cellular functions such as migration, proliferation, and differentiation. Molecules involved in cell substrate adhesion have been thoroughly studied [1] , yet quantitative experimental techniques are still needed to provide better a understanding of the mechanics of cell adhesion. In the context of atherosclerosis, the early stage of the disease involves the transmigration of monocytes in abnormally high numbers, which then accumulate in arterial walls and participate in the formation of atherosclerotic plaques [2]. Measuring changes in the adhesion of endothelial cells should help shed light on this process, as mechanical changes in endothelial cells following monocyte adhesion might play a crucial role in this pathologically high transmigration. Indeed, previous results by Kataoka *et al.* have suggested that *in vitro*, the contact between white blood cells and endothelial cells modifies the strength of endothelial cell adhesion to their substrate [3]. They found indirect evidence of a reduced adhesion in the presence of white blood cells, by measuring a change in the electrical resistance of a population of endothelial cells. They interpreted the observed decrease of electrical resistance in the presence of white blood cells as evidence of nanometer-scale increase in the distance between the ventral cell surface and the substrate. However, a more direct characterization of the mechanical properties of endothelial cells is still needed to better understand their response to leukocyte adhesion.

Although the behavior of red blood cells detaching from a surface has been experimentally and numerically investigated while monitoring the applied force [4, 5], and though several techniques exist to measure the adhesion of cells adhering weakly to a substrate or to another cell, scarce data are available on strongly adherent cells such as endothelial cells. Previous techniques at the single-cell level relied on pulling a micro- or nanoneedle inserted into the cell body [6, 7, 8], pulling [9, 10] or scraping [11, 12] the cell of interest with a bending cantilever, and aspirating the cell with a micropipette [13, 14, 15, 16].

0006-3495/08/09/2624/12 $2.00 doi: XXX/biophysj.XXX

Experiments were also carried out on cell populations, in which cell detachment was induced by centrifugation or hydrodynamic stress [17, 18], yielding ensemble-averaged values for the quantities of interest. However, some of these studies involve technical difficulties, such as the need for protein scaffolding of the cells to avoid membrane rupture when pulled by a nanoneedle [8]. Moreover, knowing the detachment force is not always straightforward. For instance, in the case of aspirating micropipettes used as cantilevers [9, 10], the detachment force measured from the cantilever deflection may not be independent of the aspiration pressure used to hold the cell and micropipette in contact, as other experiments with static micropipettes indicate that a high aspiration pressure is enough to detach a cell without having to bend the micropipette [13]. In turn, in this last work the micropipette was not held in direct contact with the cells, so that the flow of medium into the pipette is expected to have contributed to the detachment force; indeed, in a related study, this was taken into account using fluid flow simulations [16].

This work presents a new technique designed to investigate the detachment of endothelial cells adhering to a substrate. This method allows for the direct measurement of the detachment force, by placing an aspirating micropipette in contact with the surface of an endothelial cell so that a seal is formed and fluid flow into the micropipette can be neglected. We can perform detachment assays on a number of individual cells in a single experimental run, thus exploring a range of cell sizes, while imposing the micropipette diameter and the aspirating pressure rate (or loading rate). Finally, Interference Reflection Microscopy (IRM) is used to monitor the adhesion areas, as was previously done in the case of adhering blood cells [9] and tumor cells [18]. In a nutshell, this technique enables us to fully probe the influence of geometric parameters, such as cell surface, adhesion areas and micropipette size, as well as dynamical parameters such as the loading rate. Lastly, we present a minimal model that captures the features of the mechanical behavior observed in our experiments.

METHODS

Endothelial Cells

Primary bovine aortic endothelial cells (BAECs) were kindly provided by A.-C. Vion and C. Boulanger and used between passages 4 and 11. They were cultured in Dulbecco's modified Eagle's medium (Invitrogen, CA, USA) supplemented with 10% fetal bovine serum (Invitrogen) and 1% penicillin/streptomycin (Invitrogen) at 37°C with 5% CO_2. The cells were passaged three times a week and resuspended in fresh culture medium. One to two days before each experiment, the cells were trypsinated with trypLE (Invitrogen) and plated at a subconfluent density onto thin-bottom IBIDI dishes (standard bottom μ-Dish 35 mm low, IBIDI, Martinsried, Germany). In another set of experiments, the cells were grown on glass microbeads instead of a Petri dish. Typically 50 dextran Cytodex-3 microcarrier beads (Sigma-Aldrich, Taufkirchen, Germany) were first deposited at the bottom of a μ-Dish in phosphate buffer saline (PBS, Invitrogen). The PBS was then removed and $\sim$ 10000 trypsinated BAECs were introduced in the μ-Dish.

Before any experiment, a μ-Dish was brought onto the stage of the microscope, where experiments were performed at room temperature in cultured medium with added 20 mM HEPES (Invitrogen), on cells that had been plated a few hours to a few days onto the Petri dish. A dependence of the detachment force on the length of time after plating was not examined in this paper. For experiments in which the cells were exposed to cytochalasin D, the cells were incubated for 30 minutes in a solution containing 1 μg/mL cytochalasin D from Zygosporium Mansoni (Sigma-Aldrich). The solution containing the cytochalasin D was then aspirated, and fresh medium was introduced. When treated with nocodazole, cells were incubated for 1 hour in culture medium containing 10 $\mu g/mL$ of nocodazole (Sigma-Aldrich).We verified that in these conditions, microtubules were properly destabilized using a live microtubule staining (tubulin tracker green, Life Technologies).

Micropatterns

Micropatterned coverslips were prepared as described by Azioune *et al.* [19]. The coverslips were first sonicated in ethanol and plasma-treated. They were then incubated in 10 mM HEPES buffer in the presence of 0.1 mg/mL of PLL-g-PEG (Surface Solutions, Dübendorf, Switzerland). After washing with PBS and water, the coverslips were illuminated with deep UV light (UVO Cleaner) through a photomask and then incubated for one hour in 100 mM $NaHCO_3$ in the presence of 50 $\mu g/mL$ fibronectin. The cells were then plated onto the coverslips, which were mounted on magnetic chambers (Chamlide, Live Cell Instrument, Seoul, Korea) before each experiment.

Micropipette Fabrication

Borosilicate glass capillaries (1 mm OD, 0.78 mm ID, Harvard Apparatus, Holliston, MA, USA) were pulled on a P-97 micropipette puller (Sutter Instruments, Novato, CA, USA). To fabricate the micropipettes used in cell aspiration, a MF-900 microforge (Narishige, Tokyo, Japan) was used to cut the extremity of pulled capillaries to the desired diameter, ranging from 4.6 to 30 μm . The body of the micropipettes was then bent at a 45°-angle so that their extremity could be held perpendicular to the plane of cell adherence. The micropipettes used to hold the Cytodex-3 beads were fabricated in the same fashion but with a 50-μm diameter at the tip.

Microscope Setup

The setup was mounted on a TE300 inverted microscope (Nikon Instruments, Tokyo, Japan) located on an air suspension table (CVI Melles Griot, Netherlands). It was equipped with a 100x oil immersion, 1.3 NA objective for experiment monitoring (Nikon Instruments), and lower magnification objectives (40x, 20x, 10x, 4x and 2x, Nikon) for micropipette positioning. Images were acquired with a Flash4.0 CMOS camera (Hamamatsu Photonics, Hamamatsu City, Japan) controlled using the software Micromanager [20]. The experiments were performed using either brigthfield microscopy or IRM . Timelapse movies were acquired at a rate of 1 frame per second, under a 100 ms exposure time for IRM.

Interference Reflection Microscopy

In performing IRM, we used a filter cube equipped with a dual-edge dichroic mirror and a dual-band bandpass emission filter (505/606-nm BrightLine and 524/628-nm BrightLine, respectively, Semrock, Rochester, USA). As an illumination source, we used an Intensilight (Nikon Instruments) with an ND8 neutral density filter, and no excitation filter. The polarization of the incoming light was assured by the dichroic mirror, but our illumination was not strictly monochromatic due to the dual-band emission filter. Raw images were processed to remove their background using the software Image j [21]. See supplementary text for details on image processing. To validate this configuration, we tested the setup using 2.2-mm glass beads (Dominique Dutscher, Brumath, France) placed at the bottom of a Petri dish in the presence of cell culture medium (see the raw picture obtained in Figure 1A). The distance between the surface of the glass bead and the surface of the Petri dish is given by $h(d) = R - \sqrt{R^2 - d^2}$, where $R = 1.1$ mm is the radius of the bead, and d is the distance from the bead center projected on the dish plane, $0 \leq d \leq R$ (inset in Figure 1A). We measured the positions of the local intensity extrema as a fonction of h, and verified that they follow the established equation [22, 18]:

$$I = \frac{I_M + I_m}{2} - \frac{I_M - I_m}{2} \cos\left(4\pi \frac{\delta}{\lambda}\right), \tag{1}$$

where I_M and I_m are respectively the maximum and minimum intensity levels and $\delta = h(d)$ (Figure 1B). The best fit was obtained for a characteristic wavelength $\lambda = 340$ nm.

When performing experiments with continuous IRM imaging, we qualitatively observed that the illumination seemed to affect the cell mechanics. Indeed, a primary detachment event occurred during which a significant part of the cell detached, but the pipette tip then had to be slightly translated in the x-y plane in order to detach the remaining part of the cell (supp. movie 2). During our experiments under brightfield illumination, we also observed cell detachment, but no additional micropipette motion was necessary to fully detach the cells. We hypothesize that this change in cell mechanics is due to the UV light used in our IRM setup: under continuous illumination, the cells are exposed to a very large amount of UV light, which likely causes phototoxic damage. In most experiments, however, we only used IRM to take a snapshot of the adhesive areas in the initial state and thus expect cell damage to be minimal.

Micromanipulators

The microscope was equipped with a motorized micromanipulator carrying a first micropipette holder at a 45° angle, and a manual 3-axis stage linked to a UT-2 joint to orient a second micropipette holder (MP285 micromanipulator: Sutter Instruments, Novato, CA, USA; IM-H1 micropipette holders and UT-2 joint: Narishige, Tokyo, Japan; 3-axis stage: Thorlabs, Newton, NJ, USA). The first micropipette was used to aspirate adherent endothelial cells, while the other was used to hold Cytodex-3 beads.

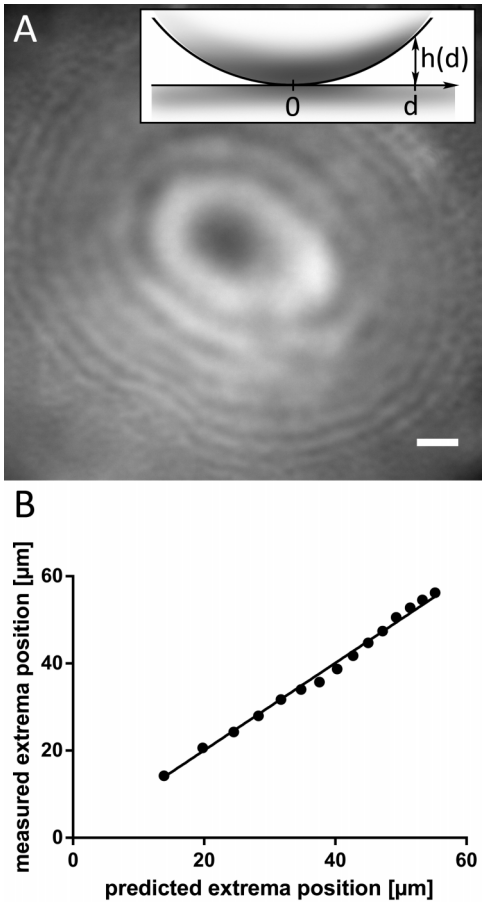

Figure 1: Determination of the IRM wavelength. *(A)* IRM picture showing the intensity minima and maxima (from destructive and constructive interference, respectively) of the light refracted from a 2.2-mm glass bead. The scale bar is 10 μm. *Inset*: In each point of the bead surface, the distance to the petri dish is $h(d) = R - \sqrt{R^2 - d^2}$, where R = 1.1 mm is the bead radius and d is the projected distance from the center of the bead. *(B)* Plot of the experimental intensity extrema positions *vs* the predictions from Equation (1) [22, 18], for λ = 340 nm. The good fit for this value of λ is evidenced by the slope of the linear regression: 1.003 ± 0.007.

RESULTS AND DISCUSSION

A constant-rate aspiration technique for cell detachment assays

We developed a new technique to apply a well-controlled aspiration force to a single endothelial cell adhering to a substrate, while quantitatively monitoring the detachment mechanics. We impose an aspiration pressure ΔP at a constant rate r_P via a micropipette held in contact with the cell body, its tip perpendicular to the substrate (Figure 2). The aspiration force applied to the cell, $F = \Delta P S_{pipette}$, is readily known, since we control both the aspiration pressure ΔP and the pipette section $S_{pipette}$. Two different setup configurations allow us to visualize and follow the detachment mechanics either in bottom or side view, which we refer to as in-plane and profile modes, respectively.

In the first configuration, or *in-plane* mode, we designed our setup in order to be able to work directly with cells cultured on the bottom of a thin-bottom Petri dish: this allows us to test a significant number of cells in a single run of experiments (up to 100/day). The Petri dish is placed above the microscope objective, parallel to the observation plane. An aspiration micropipette fabricated as described above is micromanipulated so that its tip is brought into contact perpendicularly to the luminal surface of the adherent endothelial cells, see Figure 2A and supp. movie 1. Monitoring the detachment in the substrate plane allows us to measure the projected cell area over time (see Figure 2B). Using IRM also gives access to evolution of adhesion areas (Figure 4A).

To better understand the detachment process, we performed complementary experiments in a second configuration, or *profile* mode. In this case, endothelial cells adhering to a microsphere held by a second micropipette are aspirated in a direction parallel to the observation plane, enabling us to observe the detachment from the side (see Figure 2D). More precisely, the cells were grown on 200-μm dextran Cytodex-3 microspheres initially designed to culture adherent cells in agitation. We used a 50 μm-diameter micropipette to firmly hold a Cytodex-3 bead. We positioned the bead so as to place endothelial cells perpendicular to the equatorial plane of the microsphere (inset in Figure 2D), which allowed us to visualize a single endothelial cell in profile. We then brought the aspiration micropipette into contact with the endothelial cell, perpendicular to its surface (Figure 2D-E). This visualization method does not give access to the projected cell area, but provides additional insight into the cell detachment dynamics.

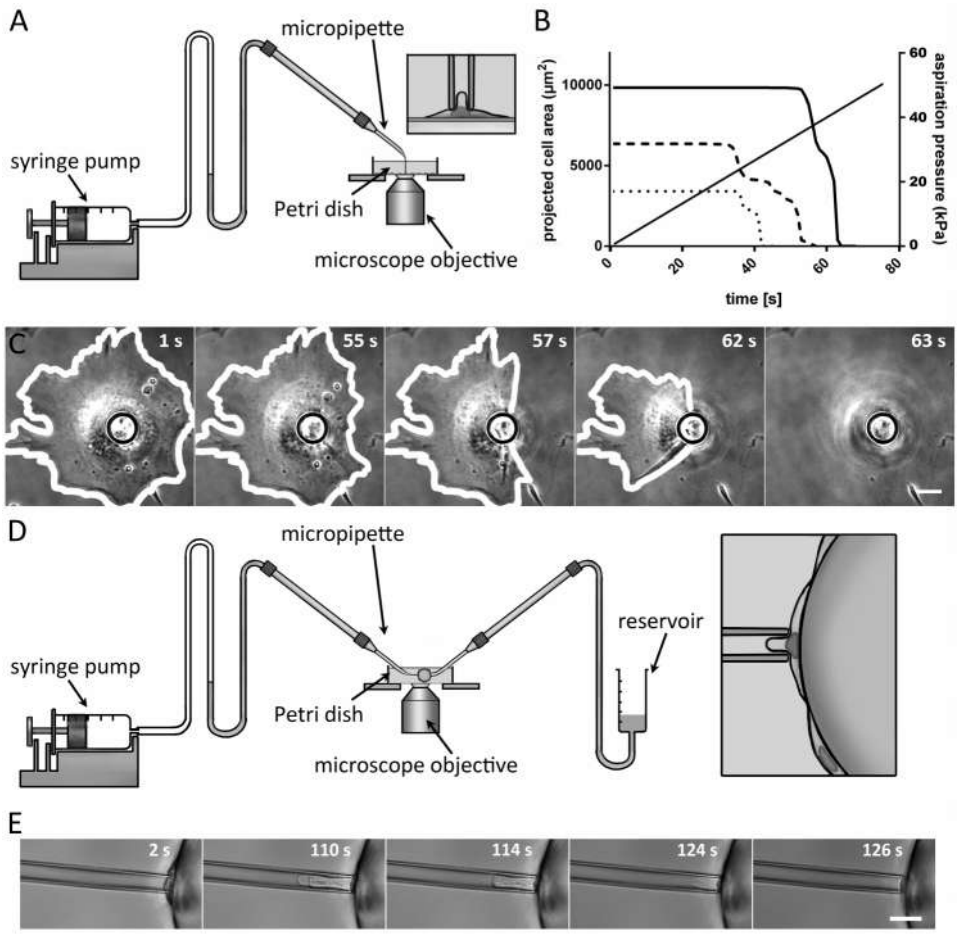

Figure 2: Setup: In-Plane *(A,B,C)* and Profile Modes *(D,E)*. *(A)* Experimental setup for in-plane aspiration experiments. In this case, the micropipette is positioned perpendicularly to the surface of adherent endothelial cells cultured on the bottom of a Petri dish. The syringe pump on the left creates a constant-rate aspiration pressure increase. *(B)* Plot of the projected cell area *vs* time for three different cells. The projected cell area is measured from pictures taken throughout the detachment. *(C)* Time-lapse of a cell throughout a detachment assay (corresponding to the solid line in *B*, and to the cell on the right in supplementary movie 1). The scale bar represents 10 μm. *(D)* Experimental setup for profile aspiration experiments. In this case, the aspiration micropipette is still positioned perpendicularly to the surface of the endothelial cells, but these adhere to a Cytodex bead, held in position by a second, larger micropipette (on the right). *(E)* Time-lapse of the detachment assay of an endothelial cell adhering to a Cytodex-3 bead. The scale bar represents 10 μm.

Detachment force and geometric parameters

The time evolution of the projected cell area is shown in Figure 2B for three different cells. Though the initial area covered by the cells varies, each case follows a qualitatively similar scenario: the projected area is constant over time until a breaking point when the projected area rapidly collapses until the cell is fully detached, at a critical aspiration pressure ΔP^*. This indicates that the detachment of cells from their substrate is a well-defined event in our assay. Moreover, for a constant micropipette diameter, we find that larger cells require a higher aspiration pressure, *i.e.* a higher aspiration force, $F^* = \Delta P^* S_{pipette}$, to detach from the substrate.

To further quantify the relation between projected area and detachment force, we performed in-plane detachment experiments on 325 cells (over several dishes and days). We found the detachment force F^* to be, at a first approximation, proportional to the initial projected cell area, S_{cell} (Figure 3A). We can then write:

$$F^* = \sigma^* S_{cell} \tag{2}$$

A linear fit of the experimental data yields a critical stress $\sigma^* = 1300 \pm 50$ Pa. All points in this dataset collapse on the master curve from Equation 2, regardless of cell size or pipette diameter. Indeed, both S_{cell} and $S_{pipette}$ vary widely here: S_{cell} ranges from 775 μm^2 to 22000 μm^2 and $S_{pipette}$ from 16.6 μm^2 to 707 μm^2 (which corresponds to pipette radii of 2.3 μm to 15 μm). Conversely, we found ΔP^* to depend on $S_{pipette}$, as shown in Figure 3B. We thus conclude that F^* is the relevant observable quantity that characterizes cell detachment, not ΔP^*.

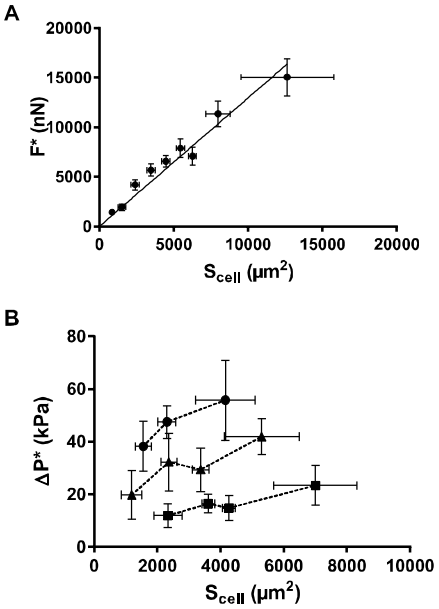

Figure 3: Critical stress. *(A)* Plot of binned experimental data showing that the detachment force scales linearly with the initial projected cell area, S_{cell}, implying that a critical stress $\sigma^* = 1300$ Pa $\pm$ 50 Pa induces cell detachment. Error bars show the standard deviation. N=335 experimental data points. (B) Critical aspiration pressure ΔP^* *vs* projected cell area for different micropipette diameters. ΔP^* depends on the micropipette section, $S_{pipette}$, used in the experiments (•: $S_{pipette} \in \left[17\ \mu m^2, 72\ \mu m^2\right]$, ▲: $S_{pipette} \in \left[78\ \mu m^2, 275\ \mu m^2\right]$, ■: $S_{pipette} \in \left[314\ \mu m^2, 707\ \mu m^2\right]$, error bars show the standard deviation.).

Since cells resist an aspiration force via cell-substrate adhesions, we used IRM to investigate the relationship between detachment force and adhesive areas at the cell-substrate interface. Indeed, these adhesive areas appear as dark patches in IRM images taken in the *in-plane* mode [18, 22, 23]. By monitoring the evolution of these adhesive areas over the duration of a complete detachment event, we found that the detachment does not occur following a peeling process occurring from the periphery but rather appeared to be initiated in the region directly under the micropipette, see supp. movie 2 and Figure 4A. These experiments lead us to assume that the adhesive areas share the pulling force throughout the aspiration assay and remain stable until rupture. However, a quantification of these experiments during the detachment process is difficult, as the

cell membrane areas that are pulled further than half a wavelength (i.e. 170 nm) away from the substrate become as dark as the adhering areas. In what follows, we consider the initial adhesive area, S_{adh}.

We relate the rupture force F^* to the initial adhesive area, S_{adh}, instead of the initial projected cell area, S_{cell}, by expressing F^* as:

$$F^* = \sigma^{**} S_{adh}, \tag{3}$$

which defines a second critical stress $\sigma^{**} = \frac{\sigma^*}{\frac{S_{adh}}{S_{cell}}}$ = 16700 ± 5600 Pa (N=16), see Figure 4B. The rupture force F^* scales with both S_{cell} and S_{adh}, and consistently, S_{cell} and S_{adh} are correlated (Spearman's correlation r=0.54, N=16 cells), with $\frac{S_{adh}}{S_{cell}}$ = 0.09 ± 0.04 (N=16 cells, mean ± SD).

The scaling of F^* with S_{adh} is easier to interpret since the resistance to the aspiration force comes from these adhesion areas. However, the correlation between S_{adh} and S_{cell} does not allow us to conclude whether S_{adh} is truly a more relevant parameter than S_{cell}. In order to constrain S_{cell}, we cultured cells on circular micropatterns of different sizes so that S_{cell} was imposed by the disk shape (S_{cell} = 520 ± 30 μm^2 on 25-μm patterns, N=12 ; S_{cell} = 760 ± 210 μm^2 on 30-μm patterns, N=10). We took advantage of the fact that S_{adh} still varied, $\frac{S_{adh}}{S_{cell}}$ = 0.16 ± 0.05 (mean ± SD), in order to study how the detachment force F^* relates to S_{adh}. Interestingly, when detaching cells from the micropatterns, F^* still scaled linearly with S_{adh} as in Equation (3), and the values obtained for the critical stress σ^{**} were comparable to those obtained without micropatterns: σ^{**} = 16700 ± 5600 Pa without a micropattern, N=16, *vs* σ^{**} = 20300 ± 5500 Pa on micropatterns, N=12. Note that in order to account for the fibronectin thickness of the micropatterns, we considered a 60 nm threshold to define the adhesion areas on the IRM pictures - instead of 50 nm on Petri dishes. Consequently, a single IRM picture of the cell-substrate interface should be sufficient to compute the aspiration force necessary to detach the cell, at a given loading rate.

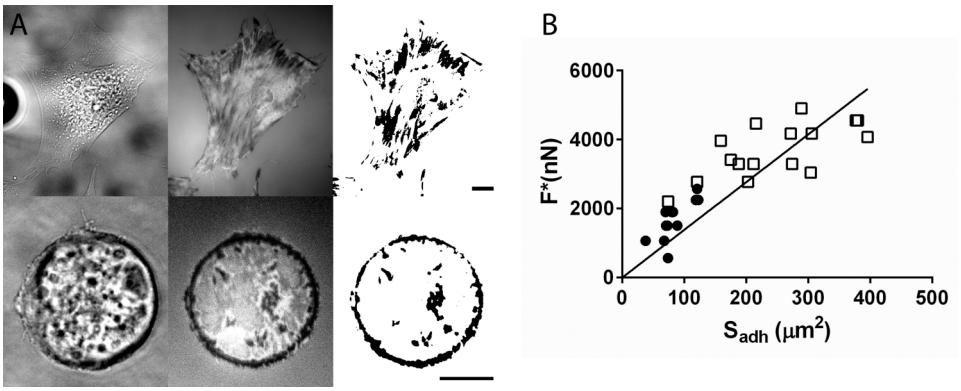

Figure 4: The detachment force scales with the adhesion area obtained from IRM images. *(A)* Each row shows from left to right: Brightfield picture, IRM picture, and binary picture showing the adhesion patches in black. Top: cell adhering to an unpatterned Petri dish. Bottom: cell constrained on a circular micropattern. The scale bars represent 10 μm. *(B)* Detachment force *vs* adhesion area. The detachment forces obtained with (•) and without (□) micropatterns scale with the adhesion area (solid line : linear fit of both datasets).

Membrane rupture does not entail cell detachment

The complete detachment process was also monitored in profile mode, in which the aspirated endothelial cell was visualized from the side under brightfield illumination (Fig. 2D-E). We found that the cell membrane appeared to break systematically before detachment (suppl. movie 3). To assess whether the membrane rupture was a triggering event for cell detachment, we performed in-plane experiments in the presence of propidium iodide in the surrounding medium. Propidium iodide is an intercaling agent that becomes fluorescent when it gains access to intracellular nucleic acids: membrane rupture is thus indicated by a sharp increase in fluorescence, see supp. movie 4. We measured the force at which the membrane broke for several pipette radii and compared it to the detachment force predicted by Equation (2) (with σ^* = 1300 Pa). This computed detachment force was systematically higher than the force at which the membrane was observed to break, *i.e.* membrane rupture always occurred before cell detachment within this range of pipette radii (Fig. 5). In profile mode, we ran a second

series of experiments in which we stopped aspirating and waited for two minutes immediately after membrane rupture. None of the 10 cells we tested detached during that period of time. At the end of this waiting period, we aspirated these cells again and verified that they could still resist a significant amount of aspiration before detaching. We ran a set of complementary experiments in in-plane mode. We applied an aspiration pressure of 5.5 kPa on cells in the presence of propidium iodide, until the rapid increase in fluorescence showed that the membrane was ruptured. As soon as rupture was detected, we set the aspiration pressure back to zero while leaving the micropipette in place, and we waited up to 300 seconds. During the whole process we imaged the cell-substrate interface with IRM at a rate of one image every 4 seconds. The quantification of these experiments showed that S_{adh} stayed relatively constant even in the presence of a broken membrane (see supplementary text, figure S3 and movie S5).

-In order to test whether detachment force would still scale with S_{cell} in absence of membrane rupture, we grew endothelial cells on a low-adhesion surface consisting of a glass coated with a low concentration of PLL-g-PEG molecules (see supplementary text). When left for 2 hours to adhere, cells developed a limited S_{cell}. Detachment force in these conditions still scaled with both S_{adh} and S_{cell} (supplementary figure S4). The critical stress σ^* = 1500 ± 500 (N= 9 cells) was very consistent with the one obtained on glass substrates, although σ^{**} = 4300 ± 2300 Pa was significantly lower (see supplementary text for further discussion).We ran another set of detachment experiments on cells grown on PLL-g-PEG in presence of propidium iodide, and they showed that for the majority of cells (15 % of N=20 cells tested), the cell membrane did not break before detachment. These sets of experiments strongly suggest that membrane rupture does not necessarily lead to cell detachment, and that it has no influence on the scaling of detachment force with cell projected area. This suggests that membrane integrity is not essential for transmitting forces to the cell-substrate interface. Considering that membrane rupture does not seem to influence the rupture force, together with our IRM observation of cells detaching first in the region directly beneath the micropipette instead of peeling from the outer rim towards the center, we concluded that the aspiration force is not transmitted to the substrate through membrane tension but rather ~~primarily through the cell cytoskeleton~~ through the whole cell body. In what follows, we then make the simplifying assumption that the adhesive bonds share the aspiration force in parallel.

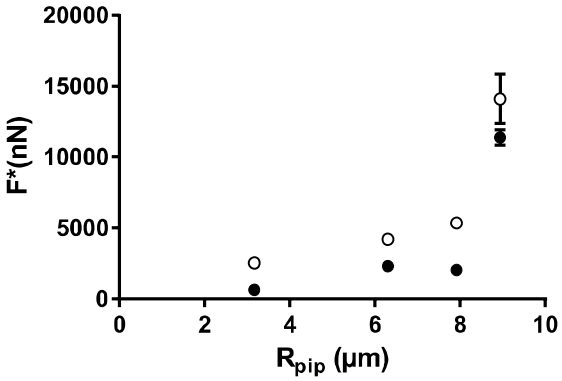

Figure 5: Aspiration force at membrane rupture and detachment force. •: force at rupture, experimental data. ◦: detachment force, predictions from Equation (2). The membrane systematically breaks before the cell detaches from the substrate. Error bars represent standard error.

Existence of intact adhesion area after cell detachment

As can be observed in movie 2, some "traces" that appear dark in IRM can be seen after cell detachment. We verified whether the presence of what we will call henceforth dark traces was systematic. Indeed, after the detachment of each of 9 cells, although these traces were hard to observe in brightfield illumination, they were systematically present in IRM (see figure S7 in supplementary text). In order to investigate the nature of the dark traces, we performed immunostaining of the substrate after cells were detached, and showed that dark traces were rich in vinculin (supplementary text and figure S8). We quantified the area S_{adh}^{after} of these dark traces, relative to S_{adh} measured before detachment. By using the same thresholding procedure of IRM images (supp. text) before and after detachment on N=13 cells, we obtained $\frac{S_{adh}^{after}}{S_{adh}}$ = 0.06 ± 0.07. Thus,

on average 94 % of all adhesive areas detach during cell detachment, so that we made the the simplifying assumption that we could neglect the potential contribution of the undetached adhesion area. However, this raised an interesting question on the process occurring locally to these remaining adhesion areas during cell detachment. One possible scenario is that at these locations, the membrane broke instead of adhesive bonds. We tried to test this hypothesis by running detachment experiments in the presence of propidium iodide while acquiring timelapses. We could not detect such local membrane rupture, and we only observed a major rupture close to the micropipette tip (as shown in supplementary movies 2 and 5). These nanoscale membrane ruptures could still exist, but get repaired too quickly [24], thus avoiding diffusion of propidium inside the cell.

Dynamic force spectroscopy of cell adhesion: cell detachment force depends on the loading rate

Since the seminal work of Evans *et al.* and further developments by other groups in the field of dynamic force spectroscopy, it has been established that when submitted to a pulling force f increasing linearly in time, a single adhesive bond breaks at a force level that is stochastic due to thermal fluctuations and that the most probable value of this rupture force, f^*, depends on the loading rate, *i.e.* the rate of force increase $\frac{df}{dt}$ [25, 26, 27, 28, 29]. All of the aspiration experiments described above were performed with an aspirating pressure increasing linearly with time, so that the aspirating force applied to the cell at any time is given by

$$F = S_{pipette}\Delta P(t) = S_{pipette} r_P t, \tag{4}$$

where $\Delta P(t)$ is the applied aspiration pressure at time t, and the aspiration rate $r_P = \frac{d}{dt}\Delta P(t)$ is the constant rate at which the aspiration pressure increases. As shown in Figure 6A, we find that the critical stress σ^* increases with the aspiration rate r_P.

Making a number of simplifying assumptions, we can write a minimal model to rationalize our experimental results for the detachment dynamics, notably the relationship between detachment force, aspiration rate and adhesive areas. As mentioned above, we first assume that the adhesive bonds share the aspiration force in parallel. Taking a mean-field approach, we assume that each adhesive bond breaks at the same rupture force f^* and approximate the number of bonds N as $N = \frac{S_{adh}}{s_0}$, where s_0 is the average area occupied by a single biological adhesive bond. Assuming a negligible transmission of the aspiration force through the membrane, a quasi-static equilibrium between the aspiration force, $F = S_{pipette}\Delta P(t)$, and the force shared by the N bonds adhering to the substrate is expressed as $F^* = Nf^* = \frac{S_{adh}}{s_0} f^*$. Note that most experiments were conducted under brightfield illumination so that we measured S_{cell} instead of S_{adh}, but as the ratio $\frac{S_{adh}}{S_{cell}}$ is well-defined, we can write:

$$\sigma^* = \frac{F^*}{S_{cell}} = \frac{S_{adh}}{S_{cell}} \frac{f^*}{s_0}, \tag{5}$$

which relates cell-scale stresses to molecular-scale forces. We further assume that for a single adhesive bond, the rupture force f^* follows a slip-bond behavior with a single energy barrier dominating its dynamics [28, 30, 31]:

$$f^* = \frac{k_B T}{x_b} \ln\left(\frac{\frac{df}{dt}}{\frac{k_B T}{x_b} k_0} \right), \tag{6}$$

where k_B is the Boltzmann constant, x_b a microscopic distance characteristic of the bond, and k_0 an off-rate (equivalently the inverse of a lifetime) under no applied force.

The loading rate of the bond is then:

$$\frac{df}{dt} = \frac{d}{dt}\left(\frac{F}{N}\right) = \frac{d}{dt} \frac{(r_P t)\, S_{pipette}}{\frac{S_{adh}}{s_0}} = r_P s_0 \frac{S_{pipette}}{S_{adh}},$$

hence:

$$\frac{df}{dt} = r_P s_0 \frac{S_{pipette}}{S_{cell}} \frac{1}{\frac{S_{adh}}{S_{cell}}}. \tag{7}$$

Combining Equations (5), (6), and (7), we obtain the master equation:

$$\sigma^* = \frac{F^*}{S_{cell}} = \frac{S_{adh}}{S_{cell}} \frac{1}{s_0} \frac{k_B T}{x_b} \ln\left(\frac{r_P \dfrac{S_{pipette}}{S_{cell}}}{\dfrac{S_{adh}}{S_{cell}} \dfrac{1}{s_0} \dfrac{k_B T}{x_b} k_0} \right), \tag{8}$$

which predicts the dependence of σ^* on S_{cell}, S_{adh}, $S_{pipette}$, r_P, and the microscopic parameters x_b, s_0 and k_0. This new expression for σ^* now captures the dependence on both the geometric parameters and r_P.

Since r_P and the pipette radius were our control parameters, we readily tested the dependency of σ^* on $\frac{S_{pipette}}{S_{cell}}$ and r_P independently. We respectively maintained r_P = 667 Pa/s constant while varying the pipette surface area from 16.6 μm^2 to 707 μm^2 (over N=335 cells), or a constant $S_{pipette}$ = 165 μm^2 while varying r_P over four different trials, r_P =167 Pa/s, 333 Pa/s, 667 Pa/s, and 1000 Pa/s (N=55 cells). Based on data from the literature [44, 35], we took $s_0 = (80\,nm)^2 = 6.4 \times 10^3\ nm^2$ for the average surface area per adhesive bond, and verified that the data satisfactorily collapsed on the master curve given by Eq. (8) (Figure 6). A linear fit of the data in Figure 6B yields a slope of 634 Pa and an intercept with the y axis, at $\ln\left(r_P \frac{S_{pipette}}{S_{cell}}\right) = 0$, of -821 Pa. Taking the average value $\frac{S_{adh}}{S_{cell}}$= 0.09 and $k_B T = 4.10^{-21}$ at room temperature, we obtain a characteristic lengthscale x_b = 0.11 nm and an off-rate k_0 = 0.006 s^{-1}. This off-rate is consistent with values obtained in single-molecule force spectroscopy: for instance, Evans *et al.* measured zero-force off-rates ranging from 10^{-4} to 10^{-1} s^{-1}. However, although a microscopic distance x_b of only 0.1 nm is not unrealistic as compared to distances measured in other bonds[32], larger microscopic distances x_b ranging from 0.4 to 0.6 nm were measured for ICAM1-β_2 integrin bonds [33, 34].

Note that to keep our model simple, we neglected the stochastic nature of the bond rupture by assuming that all bonds would all break at the most probable rupture force, f^*, and implicitly considered that once broken, adhesive bonds could not reform. However, we are applying very weak loading rates on each bond ($\sim 4.10^{-2} - 4$ pN/s) and rebinding might play a role. Litvinov *et al.* [35] found much larger off-rates for fibrinogen-integrin interactions than we did in this study, on the order of $k_0 \sim 1\ s^{-1}$. This large discrepancy with our value for k_0 could be a signature of the rebinding that we neglected in our model. Another major assumption we made was to consider slip bonds, ~~some adhesive bonds have been shown to behave as catch bonds~~ although evidence of both slip and catch bonds were reported for integrins (see [36, 37, 38, 39] for slip bonds, and more recently [40] for catch bonds). One technical advantage of considering slip bonds is that the relationship between the rupture force f^* of a single slip bond submitted to a loading rate is simple and involves only two microscopic parameters. On the other hand, there are multiple catch bonds models, and they involve more parameters [30, 41].

The master Equation (8) underestimates the detachment stress σ^* at large ~~low~~ values of $\frac{S_{pipette}}{S_{cell}} r_P$, *i.e.* at large ~~low~~ loading rates, according to Eq. (7): this might be due to our model for the dynamics of adhesive bonds, as it has been shown that the dynamics of some adhesive bonds are dictated by more than one major energy barrier [26, 28]. To take this into account, Equation (6) could be refined to include multiple linear terms in the relationship between f^* and $\ln\left(\frac{df}{dt}\right)$, with coefficients depending on the energy barrier governing the dissociation dynamics [26, 28, 29, 42]. Nevertheless, our simple model captures well the dependence on geometric parameters (S_{cell}, $S_{pipette}$, $\frac{S_{adh}}{S_{cell}}$), on intrinsic characteristics of adhesive bonds (x_b and k_0), and notably on the rate r_P at which the aspiration pressure is applied. This validates our global picture of detachment dynamics relying on adhesive areas sharing the aspiration stress in parallel.

Effect of cytoskeletal inhibitors

In order to assess the role of the cytoskeleton, we also investigated the effect of actin depolymerization. To do so, we incubated cells for 30 minutes with a high concentration of cytochalasin D (1 $\mu g/mL$). The cells affected by the drug displayed a starlike form instead of the convex polygonal shapes of untreated cells (see figure S9 in supplementary text), but showed only a slight decrease in their $\frac{S_{adh}}{S_{cell}}$ ratio in the remaining cell area($\frac{S_{adh}}{S_{cell}}$ = 0.07±0.02, N=30, in the presence of cytochalasin D, versus 0.09±0.04, N=16, without cytochalasin D). We could roughly estimate S_{cell} before treatment by measuring the surface of the convex polygon in which the cell surface is inscribed. Such a rough estimate made on 5 cells led us to assume that S_{cell} was reduced by a factor of 0.7 ± 0.1 by cytochalasin D. The fact that $\frac{S_{adh}}{S_{cell}}$ is comparable to untreated cells means that both S_{adh} and S_{cell} were affected by cytochalasin D. Interestingly, even though we again varied the aspiration rate, the measured σ^* collapsed on the same master curve defined by Eq. (8) (see figure S10 in supplementary text). We further investigated the potential role of cytoskeleton by destabilizing the microtubule network with nocodazole. We obtained an adhesion area S_{adh}

that was larger relative to S_{cell} than in the control case without nocodazole ($\frac{S_{adh}}{S_{cell}}$ = 0.17±0.09 %, N=15), consistent with the slightly higher values for σ^* than would have been predicted by the master curve for a comparable aspiration rate and pipette diameter (Fig.6B).

Comparison with other studies

Although direct comparison is not straightforward, we can place our results in the context of the literature on cell detachment. Experiments on biotinylated red blood cells adhering to streptavidin-coated surfaces [4] also lead to a detachment process in two phases. During the first phase, the contact radius slowly decreased, and then the adhesive contact underwent a "catastrophe-like" diminution until separation[4]. We do not see a slow reduction of adhesion area in our experiments, but the "catastrophe-like" diminution of adhesive area quite matches what we observe. The authors also introduced a critical force $f_c = \pi R_c W$ over which the adhesive contact cannot withstand a force in static conditions, where W is the adhesion energy per unit area and R_c the contact radius. We can then estimate a critical stress σ^* as $\frac{f_c}{\pi R_c^2} = \frac{W}{R_c} \sim \frac{10^{-4} J.m^{-2}}{10^{-6} m}$ ~100 Pa. Shortly before Pierrat *et al.*, Prechtel *et al.* [43] ran similar experiments but with vesicles decorated with lipopeptides and adhering to endothelial cells via integrins. The authors also observed the detachment of the vesicle that was very rapid (within ~ 40 msec). They performed experiments at larger loading rates than we did, but extrapolating their rupture force *vs* loading rate relationship leads to detachement forces as low as 100 pN for adhesive patches of typical radius of 1 μm, hence a critical stress of only tens of pascals. Francis *et al.*[9] used flexible aspirating micropipettes used as cantilevers to detach red blood cells and *Dictyostelium discoideum* amoeba from hydrophobic or hydrophilic substrates while using IRM to monitor the adhesion areas. For red blood cells, they obtained detachment forces of ~1 nN, for adhesion area S_{adh} ~0.3 μm^2, based on which we can estimate a critical stress σ^{**} ~ 3000 Pa. For the detachment of *Dictyostelium discoideum*, the authors found a detachment force of ~10 nN for an adhesion area ~2 μm^2, leading to a value of critical stress σ^{**} ~ 5000 Pa, close to the one they obtained with red blood cells. We have neither information on the loading rate used nor on the ratio $\frac{S_{adh}}{S_{cell}}$ in that case, but based on the figures in reference [9] we can roughly estimate $\frac{S_{adh}}{S_{cell}}$ ~0.3, so that σ^* ~ 0.3 σ^{**} ~1000 Pa. These values are larger than the one estimated above based on studies by Pierrat *et al.* and Prechtel *et al.*, but one major reason might be that the latter use specific bonds, whereas Francis *et al.* use hydrophilic or hydrophobic glass substrate with no serum in the medium (hence no extracellular matrix molecules). We stress that a difference in the red blood cell detachment is that the force is expected by the authors to act only at the perimeter of the adhesion zone, in a ring of finite width [43], as opposed to our case where force is shared by adhesive bonds in parallel. Coman used micro needles to pull on cell-cell adhesions [6, 7] and obtained typical rupture forces of 10^4 nN (1 milligram) for non tumoral cells, but without information of cell-cell adhesion area. By (roughly) estimating lateral contact between epithelial cells used by Coman as ~ 100μm^2, we obtain a critical stress estimate of 10^5 Pa, much larger than our measurements, although with no information of the applied loading rate, and the fact that we might overestimate the area and cell-cell contacts. Ryu *et al.* [8] pulled with a nanoneedle on cells covered with a proteic scaffold and obtained detachment forces of ~ 500 nN. By estimating the area of the cell-substrate interface as ~ 100μm^2, we can estimate a critical stress as ~ 5 kPa. They used nanoneedles of spring constant ~ 1 N/m, and a retraction velocity of 5 μm/s, leading to a force increasing at a rate of 5000 nN/s, that is larger than the maximal loading rate (on the whole cell) $\frac{dF}{dt} = S_{pipette} r_P$ ~ 700 nN/s that we used, making their larger critical stress value consistent with our measurements. In a different experimental configuration, Salánki *et al.* performed detachment assays using an aspirating micropipette held near (but not in contact with) an adhering cell, with a stepwise increment in aspiration pressure[16]. The detachment force was not measured but rather computed using fluid flow simulations, and they obtained typical values of 2000 nN. Their cells had a projected area of 500-700 μm^2, yielding a typical stress of 3000-4000 Pa that might be consistent with our measured critical stress σ^*. However, Salánki *et al.* did not correlate the detachment force with the cell projected area for a given cell type, so that it is difficult to speculate whether their data are directly comparable to ours regarding applied loading rate.

Regarding techniques that employ cell detachment by shear, a study using a cantilever of known stiffness to measure the force necessary to scrape cells from their substrate found a constant critical shear stress of 530-750 Pa [11, 12]. Their cantilever stiffness being 3.12 $N.m^{-1}$ and its approach velocity 20 $\mu m.s^{-1}$, the loading rate applied on the cell was ~ 6.10^4 $nN.s^{-1}$. At our highest aspiration rate r_P and our largest $S_{pipette}$, we impose a loading rate on the whole cell of $\frac{dF}{dt}$ ~ 700 $nN.s^{-1}$, which corresponds to a critical stress σ^* ~ 3000 Pa (Fig. 6B) , a larger value in comparison, even larger if we were to interpolate to a higher loading rate. Studies performed in microfluidic channels apply a fluid shear stress to a cell population. Klein *et al.*[18] increased the shear stress in a stepwise manner and measured a critical fluid shear stress of 3-4 Pa over which 50% of adhered cells would detach. Assuming that this value is representative of a critical stress obtained by shearing cells, this is very small compared to all of the previously mentioned studies, including ours. However, the authors use a model to deduce an adhesion force of ~ 200 nN and ~ 300 nN per cell for two different cell types. By dividing by the measured projected cell area of ~

300 and ~ 80 μm^2, respectively, we can estimate a critical stress of 700 and 400 Pa, respectively. It is not clear whether this critical stress is not strongly model-dependent, nor if it can considered as a critical stress that would be obtained by pulling cells, while the critical fluid shear stress of only a few Pascal is representative of the critical stress obtained by a dezipping of adhesion molecules. Finally, Christ et al.[17] measured critical fluid shear stress of 50-100 Pa.

-Overall, our measurements are in better agreement with pulling techniques [6, 7, 8, 9] than with shearing techniques [11, 12, 17, 18]. Scrapping might be more similar to a "unzipping" of the adhesion molecules on a frontline, as opposed to our situation where adhesive bond seem to withstand the pulling force in parallel.

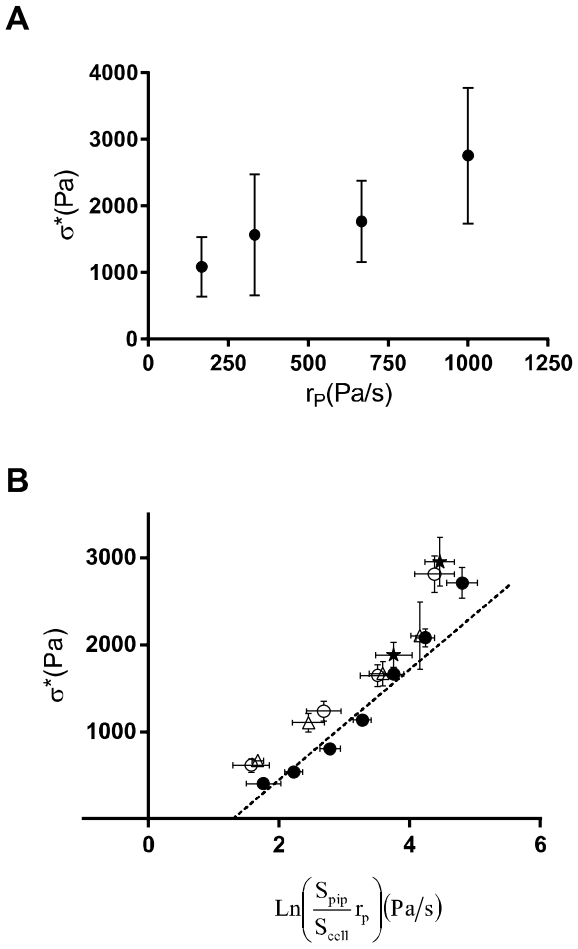

Figure 6: Critical stress as a function of the aspiration rate and master equation. *(A)* Critical stress *vs* aspiration rate, experimental data. The error bars represent the standard deviation. *(B)* Critical stress *vs* $\ln\left(\frac{S_{pipette}}{S_{cell}} r_P\right)$: ($\circ$) r_P varies while $\frac{S_{pipette}}{S_{cell}}$ is constant (data points shown in *A*); ($\bullet$) $\frac{S_{pipette}}{S_{cell}}$ varies while r_P is constant; ($\triangle$) experiments with cytochalasin D; ($\star$) experiments with nocodazole. All data collapse along the master curve, in good agreement with the prediction from Equation (8). The error bars represent the standard error.

CONCLUSION

We developed a new micropipette-based technique to quantify the adhesion force at the single cell level. This technique enabled us to fully probe the influence of geometric parameters such as projected cell area, adhesion areas and micropipette size, as well as dynamical parameters such as the loading rate. We found cell detachment to be a well-defined event, and

established a clear correlation between the detachment force and the cell adhesion area. Furthermore, we demonstrated that the detachment force is not a constant but depends on how the force is applied to the cell. Finally, a minimalist model helped us rationalize how the critical stress characterizing cell detachment depends on the cell adhesive area, intrinsic parameters of the adhesive bonds, and the rate at which the force is applied to the cell. We showed that we can predict the force necessary to detach a cell from a substrate by acquiring a single IRM picture of that cell and measuring the area covered by the adhesive bonds. In the context of leukocyte-endothelium interactions, it is therefore reasonable to postulate that the formation of micro-gaps following monocyte adhesion described by Kataoka *et al.* [3] should be detectable directly through IRM. We believe this technique should prove useful to study in detail the changes at the single endothelial cell level induced by monocyte adhesion. It would also be interesting to test how the adhesion of other leukocytes affect the mechanical properties of endothelial cells. Kang *et al.* [45] have shown that neutrophil adhesion induces a local decrease in endothelial stiffness at the adhesion point that lasts less that 1 minute, but also a stiffness increase in adjacent endothelial cells. Forthcoming results on monocyte and lymphocyte adhesion should help understand whether those changes are a universal mechanical response of endothelial cells to the adhesion of leukocytes, or whether these cells can adapt their response to the type of leukocyte adhering to them.

AUTHOR CONTRIBUTIONS

J.H. designed research; B.H., A.B., and Y.H. performed research; B.H. and J.H. analyzed data; B.H., A.I.B. and J.H. wrote the paper.

ACKNOWLEDGEMENTS

The authors acknowledge Julie Lafaurie-Janvore for introducing them to the micropatterning technique. J.H. would like to acknowledge Delphine Lhuiller, Caroline Foubert, Daniel Guy, Antoine Garcia, and Do Chi Toa Vu for technical support, and David Gonzalez-Rodriguez and Maria-Elisabetta Serrentino for fruitful discussions. This work was supported by a permanent endowment in cardiovascular cellular engineering from the AXA Research Fund.

References

[1] Zaidel-Bar, R., and B. Geiger. 2010. The switchable integrin adhesome. *J Cell Sci.*123:13851388.
[2] Ross, R. 1999. Atherosclerosis – An Inflammatory Disease. *N Engl J Med* 340:115–126.
[3] Kataoka, N., K. Iwaki, K. Hashimoto, S. Mochizuki, Y. Ogasawara, M. Sato; K. Tsujioka, and F. Kajiya. 2002. Measurements of endothelial cell-to-cell and cell-to-substrate gaps and micromechanical properties of endothelial cells during monocyte adhesion . *Proc. Natl. Acad. Sci. USA.* 99(24):15638–15643.
[4] Pierrat, S., F. Brochard-Wyart, and P. Nassoy. 2004. Enforced detachment of red blood cells adhering to surfaces: statics and dynamics. *Biophys J.* 87(4):2855–2869.
[5] Erdmann, T., and U. S. Schwarz. 2004. Adhesion clusters under shared linear loading: A stochastic analysis. *Europhys. Lett.* 66(4):603–609.
[6] Coman, D. R. 1944. Decreased Mutual Adhesiveness, a Property of Cells from Squamous Cell Carcinomas. *Cancer Res.* 4: 625–629.
[7] Coman, D. R. 1961. Adhesiveness and Stickiness: Two Independent Properties of the Cell Surface. *Cancer Res.* 21:1436–1438.
[8] Ryu, S., Y. Hashizume, M. Mishima, R. Kawamura, M. Tamura, H. Matsui, M. Matsusaki, M. Akashi, and C. Nakamura. 2014. Measurement of cell adhesion force by vertical forcible detachment using an arrowhead nanoneedle and atomic force microscopy. *Biochem. Biophys. Res. Commun.* 451:107–111.
[9] Francis, G. W., L. R. Fisher, R. A. Gamble, and D. Gingell. 1987. Direct measurement of cell detachement force on single cells using a new electromechanical method. *J Cell Sci.* 87(Pt 4):519–523.
[10] Colbert, M. J., A. N. Raegen, C. Fradin, and K. Dalnoki-Veress. 2009. Adhesion and membrane tension of single vesicles and living cells using a micropipette-based technique. *Eur Phys J E Soft Matter.* 30(2):117–121.
[11] Yamamoto, A., S. Mishima, N. Maruyama, and M. Sumita. 1998. A new technique for direct measurement of the shear force necessary to detach a cell from a material. *Biomaterials* 19:871–879.
[12] Sagvolden, G., I. Giaever, E. O. Pettersen, ans J. Feder. 1999. Cell adhesion force microscopy. *Proc Natl Acad Sci USA.* 96: 471–476.
[13] Athanassiou, G., and D. Deligianni. 2001. Adhesion strength of individual human bone marrow cells to fibronectin. Integrin β_1-mediated adhesion. *J Mater Sci Mater Med.* 12(10–12):965–970.
[14] Sung, K. L. , L. A. Sung, M. Crimmins, S. J. Burakoff, and S. Chien. 1986. Determination of junction avidity of cytolytic T cell and target cell. *Science* 234:1405–1408.
[15] Martinez-Rico, C., F. Pincet, J.-P. Thiery, and S. Dufour. 2010. Integrins stimulate E-cadherin-mediated intercellular adhesion by regulating Src-kinase activation and actomyosin contractility. *J Cell Sci.* 123:712–722.
[16] Salánki, R., C. Hõs, N. Orgovan, B. Péter, N. Sándor, Z. Bajtay, A. Erdei, R. Horvath, and B. Szabó. 2014. Single cell adhesion assay

using computer controlled micropipette. *PLoS ONE* 9: e111450.
[17] Christ, K. V., and K. T. Turner. 2010. Methods to measure strength of cell adhesion to substrates. *J Adhes Sci Technol.* 24:2077–2058.
[18] Klein, K., C. Rommel, V. Hirschfield-Warneken, and J. Spatz. 2013. Cell membrane topology analysis by RICM enables marker-free adhesion strength quantification. *Biointerphases.* 8(1):28.
[19] Azioune A., M. Storch, M. Bornens, M. Théry, and M. Piel. 2009. Simple and rapid process for single cell micro-patterning. *Lab Chip.* 9, 1640–1642.
[20] Edelstein, A., N. Amodaj, K. Hoover, R. Vale, and N. Stuurman. 2010. Computer Control of Microscopes Using μManager. *Curr Protoc Mol Biol.* 14(20):1–17.
[21] Schneider, C. A.,W. S. Rasband,K. W. Eliceiri. 2012. NIH Image to ImageJ: 25 years of image analysis. *Nat Methods.* 9, 671–675.
[22] Pierres, A., A.M. Bernoliel, and P. Bongrand. 2002. Cell Fitting to Adhesive Surfaces: A Prerequisite to Firm Attachment and Subsequent Events. *Europ Cells and Mat.* 3:31–45.
[23] Curtis, A. S. G. 1964. The Mechanism of Adhesion of Cells to Glass. A Study by Interference Reflection Microscopy. *J. Cell Biol.* 20:199–215.
[24] Andrews N. W., P. E. Almeida, and M. Corrotte. 2014. Damage control: cellular mechanisms of plasma membrane repair. *Trends Cell Biol.* 24:734–742.
[25] Evans, E., K. Ritchie, and R. Merkel. 1995. Sensitive Force Technique to Probe Molecular Adhesion and Structural Linkages at Biological Interfaces. *Biophys J.* 68:2580–2587.
[26] Merkel, R., P. Nassoy, A. Leung, K. Ritchie, and E. Evans. 1999. Energy landscapes of receptor-ligand bonds explored with dynamic force spectroscopy. *Nature* 397(6714):50–53.
[27] Dudko, O. K., A. E. Filippov, J. Klafter, and M. Urbakh. Beyond the conventional description of dynamic force spectroscopy of adhesion bonds *Proc Natl Acad Sci USA.* 100(20):11378–11381.
[28] Pincet, F., and J. Husson. 2005. The solution to the streptavidin-biotin paradox: the influence of history on the strength of single molecular bonds. *Biophys J.* 89(6):4374–4381.
[29] Husson, J., and F. Pincet. 2008. Analyzing single-bond experiments: influence of the shape of the energy landscape and universal law between the width, depth, and force spectrum of the bond. *Phys Rev E Stat Nonlin Soft Matter Phys.* 77:026108.
[30] Evans, E., A. Leung, V. Heinrich, and C. Zhu. 2004. Mechanical switching and coupling between two dissociation pathways in a P-selectin adhesion bond. *Proc Natl Acad Sci USA.* 101(31):11281–11286.
[31] Dembo, M., D. C. Torney, K. Saxman, and D. Hammer. 1988. The reaction-limited kinetics of membrane-to-surface adhesion and detachment. *Proc R Soc Lond B Biol Sci.* 234:55–83.
[32] R. Merkel. 2001. Force spectroscopy on single passive biomolecules and single biomolecular bonds. *Phys. Rep.* 346, 343–385.
[33] Evans, E., K. Kinoshi, S. Simon, and A. Leung. 2010. Long-Lived, High-Strength States of ICAM-1 Bonds to β_2 Integrin, II:Lifetimes of Bonds to Recombinant $\beta_L\beta_2$ Under Force *Biophys J.* 98(8):1458–1466.
[34] Kinoshita, K., A., Leung, S. Simon, and E. Evans. 2010. Long-Lived, High-Strength States of ICAM-1 Bonds to β_2 Integrin, II:Lifetimes of LFA-1 Bonds Under Force in Leukocyte Signaling *Biophys J.* 98(8):1467–1475.
[35] Litvinov, R. I., A. Mekler, H. Shuman, J. S. Bennett, V. Barsegov , and J. W. Weisel. 2012. Resolving Two-dimensional Kinetics of the Integrin αIIbβ3-Fibrinogen Interactions Using Binding-Unbinding Correlation Spectroscopy.*J Biol Chem.* 287:35275–35285.
[36] Zhang, X., E. Wojcikiewicz, and V. T. Moy. 2002. Force Spectroscopy of the Leukocyte Function-Associated Antigen-1/Intercellular Adhesion Molecule-1 Interaction. *Biophys J.* 83:2270–2279.
[37] Zhang, X., A. Chen, D. De Leon, H. Li, E. Noiri, V. T. Moy, and M. S. Goligorsky.2004. Atomic force microscopy measurement of leukocyte-endothelial interaction. *Am J Physiol Heart Circ Physiol.* 286:H359–H367.
[38] Li F., S. D. Redick, H. P. Erickson, and V. T. Moy. 2003. Force Measurements of the $\alpha_5\beta_1$ IntegrinFibronectin Interaction. *Biophys J.* 84:1252–1262.
[39] Jiang, G., G. Giannone, D. R. Critchley, E. Fukumoto, and M. P. Sheetz. 2003. Two-piconewton slip bond between fibronectin and the cytoskeleton depends on talin. *Nature* 424:334–337.
[40] Kong, F., A. J. García, A. P. Mould, M. J. Humphries, and C. Zhu. 2009. Demonstration of catch bonds between an integrin and its ligand. *J Cell Biol.* 185:1275–1284.
[41] Pereverzev, Y. V., O. V. Prezhdo,M. Forero,E V. Sokurenko, and W. E. Thomas. 2005. The Two-Pathway Model for the Catch-Slip Transition in Biological Adhesion. *Biophys J.* 89:1446–1454.
[42] Bartolo, D., I. Derényi, and A. Ajdari. 2002. Dynamic response of adhesion complexes: Beyond the single-path picture.*Phys. Rev. E* 65:051910.
[43] Prechtel, K. A., R. Bausch, V. Marchi-Artzner, M. Kantlehner, H. Kessler, and R. Merkel. 2002. Dynamic Force Spectroscopy to Probe Adhesion Strength of Living Cells. *Phys Rev Lett.* 89(2):028101.
[44] Selhuber-Unkel, C., M. López-García, H. Kessler, and J. P. Spatz. 2008. Cooperativity in Adhesion Cluster Formation during Initial Cell Adhesion. *Biophys J.* 95:5424–5431.
[45] Kang, I., Q. Wang, S. J. Eppell, R. E. Marchant, and C. M. Doerschuk. 2010. Effect of Neutrophil Adhesion on the Mechanical Properties of Lung Microvascular Endothelial Cells. *Am J Respir Cell Mol Biol.* 42:591–598.

SUPPORTING MATERIALS

An online supplement to this article can be found by visiting BJ Online at http://www.biophysj.org.

List of Figures